Determination of the Region of No Effect of the Notch on Fatigue Life of Aa2519 T62 Aluminium Alloy

Maciej Kotyk[1*], Przemysław Strzelecki[1]

[1] Bydgoszcz University of Science and Technology, ul. Profesora Sylwestra Kaliskiego 7, 85-796 Bydgoszcz, Poland
* Corresponding author's e-mail: mackot001@pbs.edu.pl

ABSTRACT

The paper presents a fatigue test of AA2519 T62 aluminium alloy in high-cycles region for smooth and notched specimens with stress concentration factors 1.75 and 2.28 for radii r1 = 2 mm and r2 = 1 mm, respectively. A number of cycles with no notch effect was determined for each notched specimens. The estimated values were compared with the distribution estimated on the literature data. Based on this knowledge, an analytical-experimental method was proposed to determine S-N curves for notched elements for aluminium alloys. The verification of the method gives satisfactory results. Additionally, the FITNET method and the Lee and Taylor method were used for comparison. The proposed method got the best results. The FITNET method and Lee and Taylor method obtained overestimated fatigue life and it can be concluded that the analytical method presented methods are suitable for steel materials. The proposed method can be used by engineers.

Keywords: stress concentration factor, high-cycle fatigue, effect of the notch, fatigue life model, number of cycles with no notch effect.

INTRODUCTION

The issue of fatigue life is inextricably linked to the design process of technical objects. The aforementioned life represents a kind of compromise between commercial profit and product features that are determined by the user, including the maximum lifetime of the object. Durability issues take on great importance when they have to do with safety, especially when operating objects moving at high speeds, such as airborne vessels, or objects whose damage will occur at a considerable distance from a facility that can provide assistance, as is sometimes the case during deep-sea shipping voyages.

The examples given are extreme cases of technical objects, but the issues related to attempts to predict the fatigue life of machinery in operation see the unwavering interest of users of objects whose damage is associated with a different degree of disaster risk. The elements that make up the technical object are for the most part not fragments of a single, flat sheet. They are usually given a varied geometry and are often varied by shaping connecting elements in them, such as holes for pins and screws. All kinds of discontinuities in the material structure represent geometric notches that significantly affect the fatigue life of these objects. Accordingly, it was deemed reasonable to determine the effect of notch action for the infrequently used material, which is an aluminium alloy with the designation AA2519, and to determine the area of fatigue life in the *S-N* curve, for which the described notch has no effect on fatigue life. To delineate the aforementioned region of no notch effect, the following train of thought was used.

Figure 1 presents a studyflow for determining fatigue characteristics for notched elements based on fatigue characteristics for smooth specimens (1–4). Practical application of this method is presented, among others, in paper (5), where the determination of *S-N* characteristics for sintered rhenium based on the monotonic properties of the material was analysed. In general, N_3 equal to 10^3

cycles is taken as the limit point indicating the area of no effect of notch action (6) and presented in newly version in (2) – named Lee and Taylor's method. This value articles well for steel materials. A different approach can be found in the paper (7), which presents the assumption that the intersection point (N_3, σ_3) is for the point $(1, S_f)$, where S_f is equal to the actual breaking stress during the monotonic tensile test. Another approach is proposed in FITNET procedure (8) where S-N curve is determine based on the point (N_z, Z) and slope coefficient m_g and m_k equal 8 and 3 for normal stress, respectively. On the other hand, in paper (9) Łagoda et al. conclude that there is no range of no notch effects on fatigue life for aluminium alloys and the characteristics for the material and notched specimens intersect outside the region that makes physical sense (for values less than 1 cycle in the S-N curve).

Due to these ambiguities and the small number of scientific reports on AA2519 material, it was decided that the purpose of this paper was to determine the intersection of fatigue characteristics for smooth and notched specimens and to present a high-cycle life model for aluminium alloys including AA2519 T62 alloy.

The same value of the number of cycles leading to failure, for the same load (stress amplitude S_a at the same value of the cycle asymmetry factor R), but different specimen geometries in this paper will be understood as the extent of the lack of influence of notch effect on fatigue life. In the diagram shown in Figure 1 point (N_3, S_3) is the boundary of the said region. This is important in

the context of determining fatigue characteristics for notched specimens with geometries other than those for which results are presented in this article. Additionally, it was proposed own method to determine S-N curve based on fatigue properties of smooth specimens.

MATERIAL AND METHODS

Material

Engineering objects, despite their wide variation mainly by purpose, have some things in common. During construction, the aim is for the designed object to be characterized by the lowest possible mass, without sacrificing mechanical properties such as stiffness or ability to carry service loads. In certain applications such as aerospace, the issue described is of particular importance, mainly because of the energy intensity of aircraft, which need to be accelerated to much higher speeds than the means of transport involved in vehicular traffic.

A historical breakthrough of sorts in the selection of engineering materials that take into account the more favourable density-to-strength ratio with respect to steel was the development by Alfred Wilm of the first duralumin (10). This later contributed to the development of advanced lightweight aerospace structures (11), including those of a military nature (12). An interesting material in this group due to technological and mechanical properties such as high specific
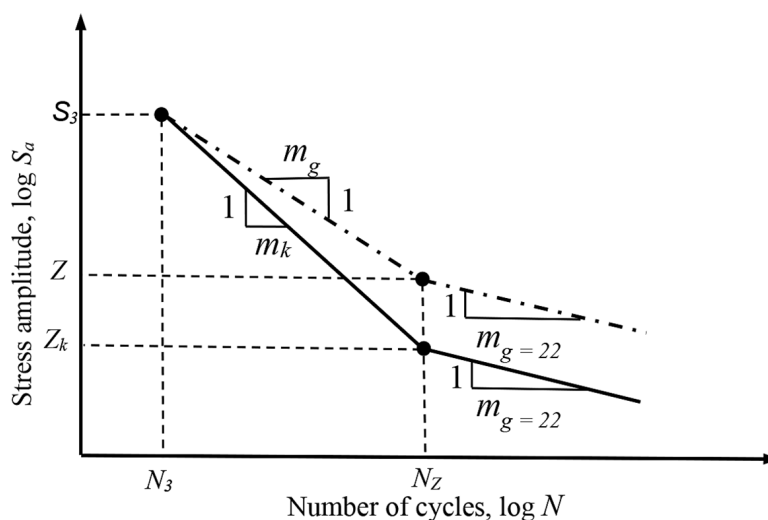
Figure 1. Methodology for determining the fatigue characteristics for a structural member (solid line) from the fatigue characteristics of the material (dot-and-point line)

strength, ballistic resistance and resistance to stress corrosion cracking is alloy AA2519, the chemical composition of which is shown in Table 1 (13–19) and the basic mechanical properties determined by monotonic tensile testing are included in Table 2. The aforementioned mechanical characteristics and the development of welding technology for sheets made from this series have made it a material that can be successfully used in light armoured vehicles and aviation (20). Due to the significantly lower density of this alloy relative to steel, aircraft armour was considered to be made from this material (21).

Based on the small number, relative to other 2XXX grade materials, of scientific reports on this material, it can be concluded that wider use of this alloy has been abandoned, or has been kept secret due to the nature of military applications. Nowadays, this material is used in the construction of composites. One of them is this one, composed of Ti6Al4V titanium alloy, a buffer layer made of AA1050 alloy and a second base layer made of the AA2519 alloy described above. The emergence of this composite has provoked increased interest in this particular lightweight alloy. However, it is not widely reported in the literature. Therefore, as previously mentioned, it was decided to extend the state of the art on the high-cycle fatigue life of AA2519 duralumin and to supplement it with a computational model to predict the effect of notching on the reduction of AA2519 high-cycle fatigue life.

The largest group of scientific literature reports found relating to the described alloy mainly concerned the tensile strength of the described dural. Depending on the variant of heat treatment, technological treatments and other factors, information about their influence on the AA2519's short-term tensile strength can be found in papers (22–25).

Due to the distinctive corrosion resistance of this type of material, some of the scientific papers found were concerned with studies of this very feature. Information regarding the effects of welding and the corrosive environment on selected mechanical properties of AA2519 alloy under selected conditions can be found in papers (26–28). Information was also encountered regarding the effect of the cooling medium during heat treatment on the corrosion resistance of the analyzed alloy (29) as well as testing of corrosion resistance when the material had galvanic layers on it (30, 31).

During the analysis of the literature on the subject of this paper, many articles discussing unusual methods of joining AA2519 alloy including by friction welding were encountered. These studies were mainly concerned with the effect of technological parameters on the joint strength (32–35). The previously mentioned difficulties in the plastic processing of this material naturally led to the interest of researchers in the direction of learning about the influence of plastic processing (mainly rolling) on selected properties of the analysed material. Examples of such papers include (36–46).

In the publicly available literature, quite a few papers have been encountered that describe the mechanical characteristics of this alloy. Those found included research information from at least several areas. Fracture mechanics was also one of them. In article (47) this very topic was addressed. The fracture toughness of this material was also the subject of the paper (48). Particularly noteworthy is the publication made by NASA (49), where a report on the fracture toughness of a wide group of materials including AA2519 is presented. Due to the specifics of the present article, during the analysis of the literature, special emphasis was placed on scientific reports treating the fatigue strength of the AA2519 alloy under study. This topic has been addressed at least several times by scientific teams from around the world. A team of researchers coordinated by R. Kosturek placed special emphasis on the influence of FSW technology on the low-cycle durability of the joint made by the FSW method, which they described very extensively in papers (50–52). An attempt

Table 2. Selected tensile properties of aluminium alloy AA25196-T62

σ_y	σ_u	E	A_5
MPa	MPa	GPa	%
353	475	67.5	16.3

Note: σ_y – yield strength, σ_u – ultimate tensile strength, E – Young's modulus, A_5 – elongation at break.

Table 1. Chemical composition of AA2519 alloy

Si	Fe	Cu	Mg	Zn	Ti	V	Zr	Al
0.06	0.08	5.77	0.18	0.01	0.04	0.12	0.2	Balance

has also been made to describe the low-cycle life of extruded profiles made from this material (53). Studies on the fatigue life of this material were also presented in an article (54), however, they were only of a comparative nature.

Based on the analysis of the literature on AA2519 alloy carried out, it can be concluded that it is difficult to find information on the high-cycle durability of AA2519 alloy in the publicly available literature. Therefore, the authors of the present paper found it reasonable to carry out the scientific article to develop a material model for AA2519 alloy and extend it to include issues related to the change in fatigue life due to the notch effect.

Methods

In order to determine the high-cycle material model, and the effect of notch on the described high-cycle durability (HCF), the following test procedure was developed and implemented. Suitable specimens were cut from a sheet of flat rolled sheet AA2519 by electro-erosion. Later, they were heat treated and artificially aged to meet the objectives of the heat treatment designated T62.

The own research consisted of determining the high-cycle fatigue life of AA2519 aluminium alloy heat-treated to T62 state, with force control. A single-axis Instron 8502 hydraulic testing machine was used to realize the load. Two assumptions were made during the implementation of the study. The first was to keep the value of the cycle asymmetry factor constant $R = -1$, and the second was that the stress values were determined nominally, without taking into account the stress concentration factor. Three specimen geometries, prepared in accordance with the recommendations of ISO 1099:2017, were

specified to perform the tests (55). The first was flat hourglass specimens with a smooth transition evenly distributed over the measuring part (no notch – smooth). In the other two specimen geometries, symmetrical notches were made on both sides so that the bottom of the mechanical notch had a radius of $r_1 = 2$ mm and $r_2 = 1$ mm. The assumed geometry was obtained with an EDM machine, using 0.25 mm diameter wire. Drawings showing the basic dimensions, as well as a photograph of already cut specimens, are presented in Figure 2. One of the specimens involved in the test, mounted in the jaws of the INSTRON 8502 single-axis hydraulic testing machine is shown in Figure 3.

Because the stresses were determined nominally, they did not reflect the actual stresses in the specimens with r_1 and r_2 radii in particular. Accordingly, it was decided to determine the stress in the roof of the notch taking into account the stress concentration factor using two methods, i.e. analytical and numerical. Form factor K_t was calculated analytically based on Noda's formulas presented in the paper (56). The K_t values for the notched specimens were 1.75 and 2.28 for radius $r_1 = 2$ mm and $r_2 = 1$ mm, respectively. To verify these calculations, FEM calculations were performed, the results of which are shown in Figure 4. The value of the axial load was assumed to be 2500 N, which corresponded to 100 MPa of nominal stress. HEX20-type elements with node counts of 29216, 32837, 32891 and element counts of 6090, 7200, and 7220 were used to prepare the specimen model for smooth and notched specimens $r_1 = 2$ mm and $r_2 = 1$ mm, respectively. The results of analytical and FEM calculations give similar values (the difference at the second decimal place).
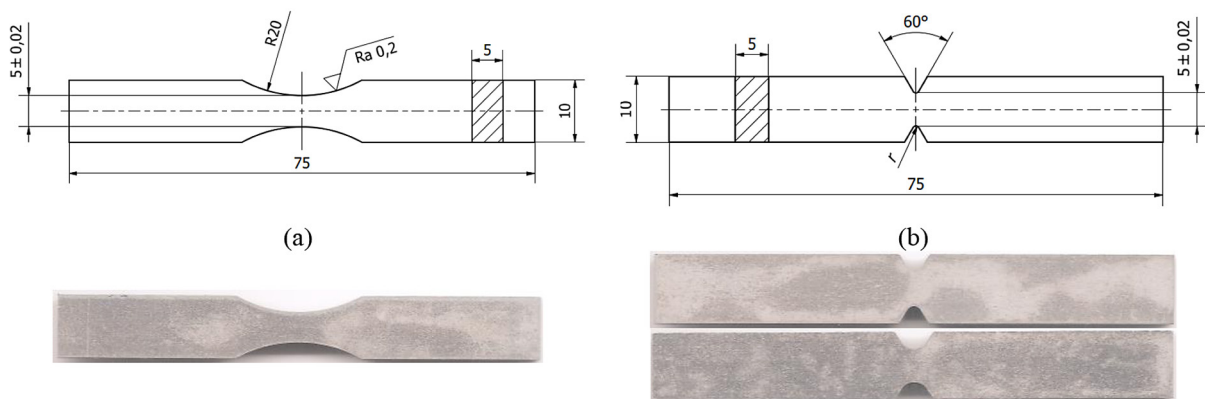
Figure 2. Geometry of specimens used for testing (a) smooth specimen, (b) notched specimens – $r_1 = 2$ mm and $r_2 = 1$ mm
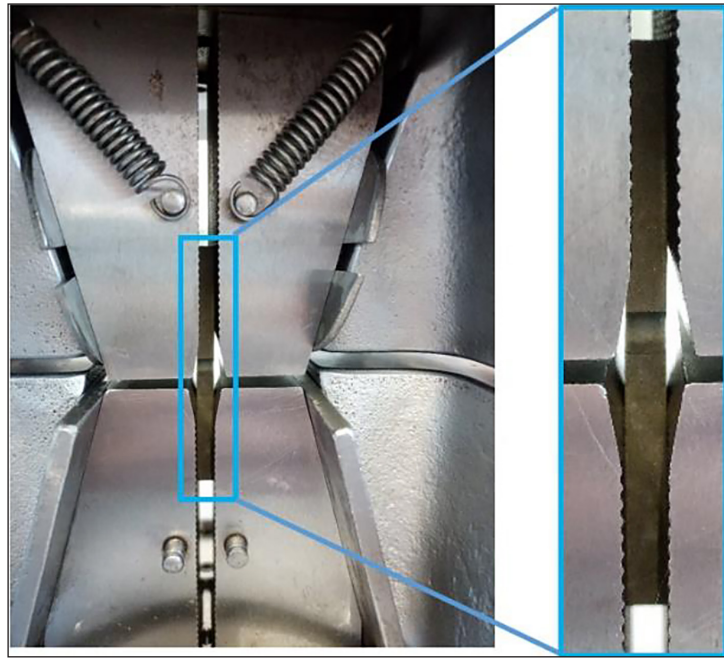
Figure 3. Specimen clamped in the jaws of the testing machine
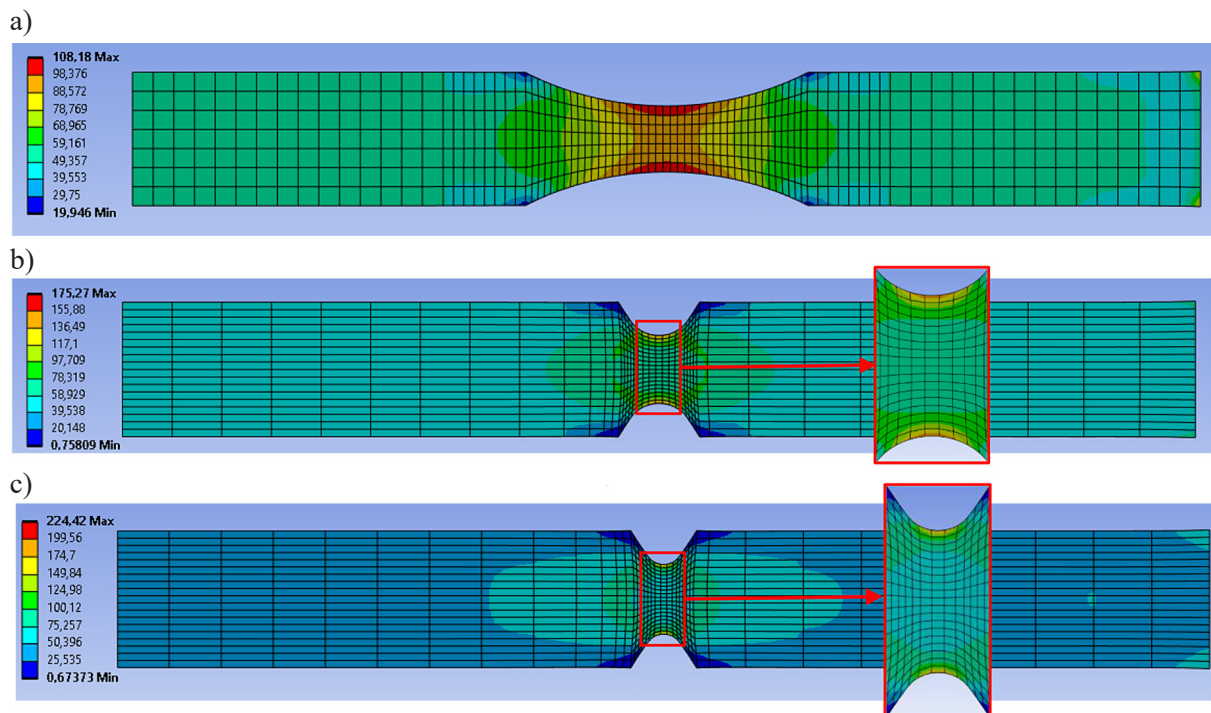
Figure 4. Results of FEM calculations for an axial load of $F = 2500$ N – nominal stress equal to 100 MPa(a) smooth specimen, (b) notched specimen – $r_1 = 2$ mm and (c) notched specimen – $r_2 = 1$ mm

VALUE OF THE NUMBER OF CYCLES FOR NO EFFECT OF THE NOTCH

To analyze the value of the number of cycles N_3 for the intersection of the characteristic approximation line for smooth specimens and the approximation line for notched specimens, literature data were used for the following aluminium alloys: 2024-T3, 2024-T4, 2024-T5, 2124-T851, 2124-T852, 2124-T853, 6061-T6, 6063-T6, 7050-T614, 7050-T7451, 7075-T6, 7075-T6, 7075-T6, 7075-T6, 7075-T651, A02950-T6 (57–64) – data presented in Table 3. In the end, 37 values relating directly to the high-cycle durability determined

Table 3. Data source used

Source	Material	N_3	K_t
Strzelecki (63)	6063-T6	3.23	1.60
Strzelecki (63)	6063-T6	4967.75	2.00
Strzelecki (63)	6063-T6	1988.17	2.60
Illg (61)	2024-T3	0.25	2.00
Illg (61)	2024-T3	0.25	4.00
Illg (61)	7075-T6	6.04	2.00
Illg (61)	7075-T6	0.25	4.00
Papuga et al. (62)	2124-T851	3.00	2.11
Papuga et al. (62)	2124-T851	0.25	2.19
Papuga et al. (62)	2124-T851	0.25	2.51
Papuga et al. (62)	2124-T852	226.31	2.42
Papuga et al. (62)	2124-T853	151.48	2.89
Bennett & Weinberg (64)	2024-T4	0.25	1.40
Bennett & Weinberg (64)	2024-T4	0.25	1.79
Bennett & Weinberg (64)	7075-T6	97.49	1.40
Bennett & Weinberg (64)	7075-T6	5.02	1.79
Bennett & Weinberg (64)	6061-T6	0.25	1.40
Bennett & Weinberg (64)	6061-T6	0.44	1.79
Antunes et al. (57)	7050-T7451	62.14	3.14
Antunes et al. (57)	7050-T614	0.25	3.14
Chaves et al. (59)	7075-T6	207.13	2.57
Chaves et al. (59)	7075-T6	4557.29	2.19
Chaves et al. (59)	7075-T6	37.69	1.78
Grover et al. (60)	2024-T3	1002.37	2.00
Grover et al. (60)	2024-T3	0.25	2.80
Grover et al. (60)	2024-T3	234.98	1.50
Grover et al. (60)	2024-T3	261.53	2.00
Grover et al. (60)	2024-T3	0.25	4.00
Grover et al. (60)	2024-T3	0.25	5.00
Grover et al. (60)	2024-T4	6.69	2.00
Grover et al. (60)	2024-T5	0.98	4.00
Grover et al. (60)	7075-T6	5.36	2.00
Grover et al. (60)	7075-T6	0.58	2.20
Grover et al. (60)	7075-T6	0.79	2.40
Grover et al. (60)	A02950-T6	39041.76	2.00
Benedetti et al. (58)	7075-T651	171.87	1.53
Benedetti et al. (58)	7075-T651	5.78	2.33

for smooth specimens and notched specimens made of previously indicated materials were obtained. The values of form factors K_t ranged from 1.4 to 5. Analysis of these data showed that the value of point N_3 is not dependent on form factor K_t, but is a random variable that cannot be linked to material type or mechanical properties. The fatigue characteristic intersection values obtained had a range of 1 ÷ 39,042 cycles. This provides a basis for rejecting the claim of Łagoda et al. (9) on the lack of the region of the no effect of the notch on the high-cycle fatigue life of aluminium alloys. On the basis of literature data, and our own research, it can be concluded that for some aluminium alloys, the fatigue strength for one load cycle is equal to the value obtained during monotonic tensile testing. A histogram of the analysed values is shown in Figure 5. Four distributions were used to describe the probability of acceptance
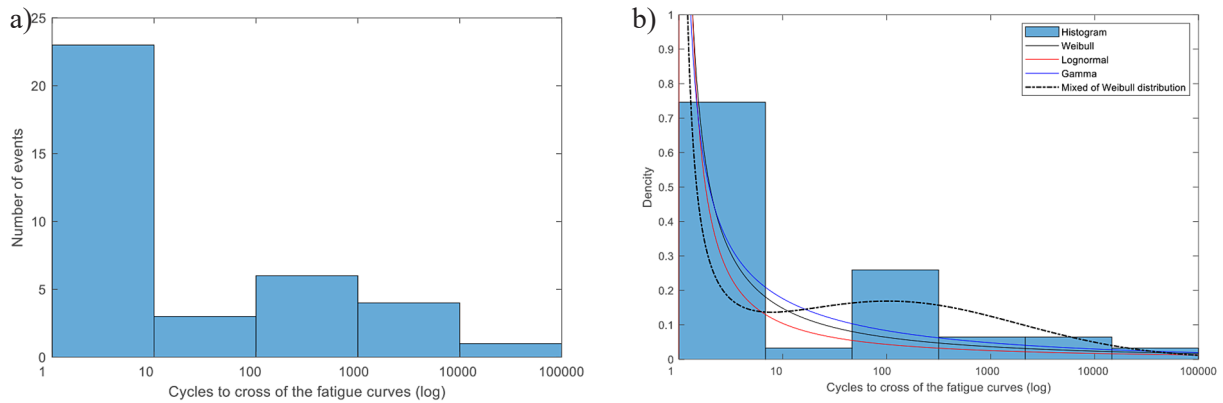
Figure 5. Histogram of fatigue characteristic intersection values for smooth and notched specimens (a) histogram for aluminum alloys, (b) histogram with probability distributions used

of fatigue characteristic lines determined for smooth and notched specimens at the hypothetical point N_3: Weibull, lognormal, Gamma and Mixtured Weibull. Descriptions of these distributions are given by mathematical formulas 1, 2, 3 and 4 (65–67), respectively.

$$f(x) = \frac{\alpha}{\beta}\left(\frac{x}{\beta}\right)^{\alpha-1} \exp\left\{\left(\frac{x}{\beta}\right)^{\alpha}\right\} \quad (1)$$

$$f(x) = \frac{1}{x\sqrt{2\pi\sigma_x^2}} \exp\left(\frac{-(\log x - \mu_x)^2}{2\sigma_x^2}\right) \quad (2)$$

$$f(x) = \frac{x^{a-1}}{b^a \cdot \Gamma(a)} \cdot e^{\frac{-x}{b}} \quad (3)$$

$$f(x) = \sum_{i=1}^{m} p_i\left[\frac{\alpha_i}{\beta_i}\left(\frac{x}{\beta_i}\right)^{\alpha_i-1} \exp\left\{\left(\frac{x}{\beta_i}\right)^{\alpha_i}\right\}\right] \quad (4)$$

where: x – $\log(N_3)$, α – shape parameter, β – scale parameter, μ_x – average value, σ_x – standard deviation, λ – scale parameter, k – shape parameter, $\Gamma()$ – Euler function, p_i – weight of *i-th* distribution, m – number of assumed distributions.

The parameters of the distributions were obtained using the maximum likelihood estimation method. For the three basic functions, the formulas of the reliability function are well known and there are no problems with their estimation. On the other hand, for the function according to formula 4 the following equation was used (67):

$$L(\theta) = \prod_{i=1}^{n}\sum_{i=1}^{m} p_i\left[\frac{\alpha_i}{\beta_i}\left(\frac{x}{\beta_i}\right)^{\alpha_i-1} exp\left\{\left(\frac{x}{\beta_i}\right)^{\alpha_i}\right\}\right] \quad (5)$$

After taking the logarithm, we get the following formula:

$$\mathcal{L}(\theta) = \sum_{i=1}^{n} \log\left\{\sum_{i=1}^{m} p_i\left[\frac{\alpha_i}{\beta_i}\left(\frac{x}{\beta_i}\right)^{\alpha_i-1} \exp\left\{\left(\frac{x}{\beta_i}\right)^{\alpha_i}\right\}\right]\right\} \quad (6)$$

To find the minimum relationship (6), a genetic algorithm of the Matlab program was used (68). A χ^2 test was used to evaluate which distribution best describes the values shown in Figure 5b. The calculations were made according to the following formula (65, 66, 69):

$$\chi^2 = \sum_{i=1}^{k} \frac{(n_i - n \cdot p_i)^2}{n \cdot p_i} \quad (7)$$

where: k – number of intervals, i – *th* interval, n_i – size for *i-th* interval, p_i – probability of occurrence of variable in *i-th* interval, n – size of all measurements.

See Table 4 for calculation results. The mixtured Weibull distribution received the largest value, so it will be used in further analyses.

Figure 6 shows the mixtured Weibull distribution along with the bi-parametric Weibull distribution (shown for comparison purposes only). The former obtained the highest *p–value*. This is due to the fact that the obtained N_3 values are bi-modal, that is, two values occur in it the most often. The distribution according to the formula 4 was written with the estimated coefficients using the relationship (8). For the data analyzed, the mixtured Weibull distribution was assumed to consist of double two-parameter Weibull distributions. In addition, Fig. 6 shows separately the members of the distribution from the formula (8). The value of coefficients p_1 and p_2 determines the weight of each member. The average value for the first member is 5, while the second is 403.

Table 4. Values of the coefficients of distributions and p-value for the χ^2 test

Distribution	Value of the coefficients						p – value
Weibull	α	0.42	β	0.53	-	-	0.0008
Lognormal	μ_x	-2.07	σ_x	3.03	-	-	$2.9 \cdot 10^{-7}$
Gamma	a	0.31	b	3.68	-	-	0.0163
Mixtured Weibull	α_1	0.39	β_1	0.12	p_1	0.59	0.0733
	α_2	2.43	β_2	2.66	p_2	0.41	
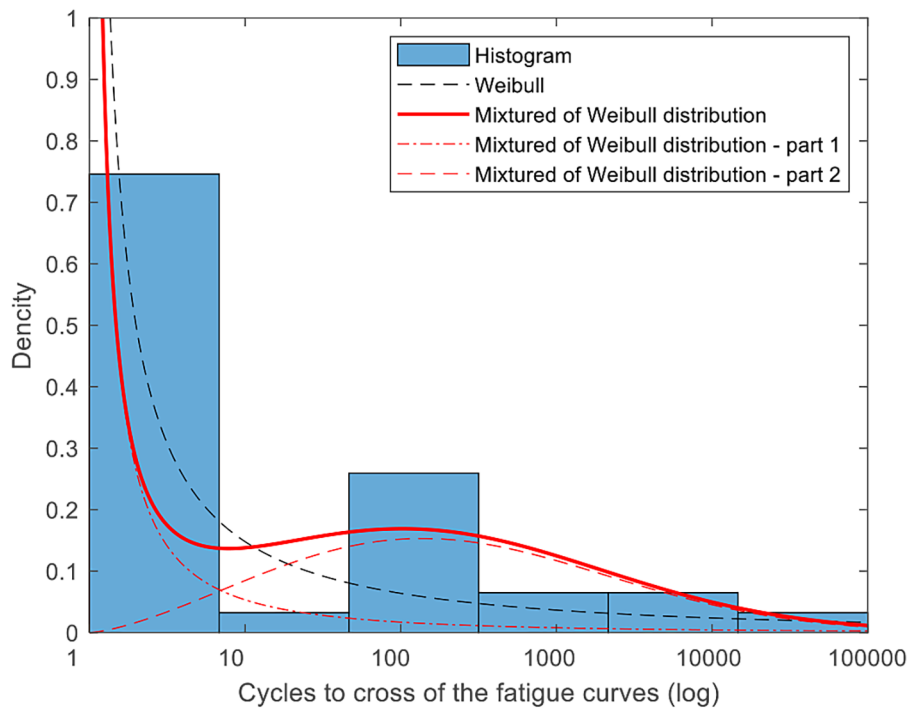
Figure 6. Histogram of fatigue characteristic intersection values for smooth and notched specimens with Weibull distributions – two-parametric (black line) and combined two-component (red line)

$$f(x) = 0.59\left[\frac{0.39}{0.12}\left(\frac{x}{0.12}\right)^{0.39-1} \exp\left\{\left(\frac{x}{0.12}\right)^{0.39}\right\}\right] + \\ + 0.41\left[\frac{2.43}{2.66}\left(\frac{x}{2.66}\right)^{2.43-1} \exp\left\{\left(\frac{x}{2.66}\right)^{2.43}\right\}\right] \quad (8)$$

It was decided to compare the obtained test results with other high-cycle durability results obtained for selected engineering materials. Fig. 7 shows the Weibull distributions for the value of the number of cycles at which the intersection point of the N_3 fatigue characteristic line for aluminium alloy and steel will occur, obtained from the literature analysis. The distribution for steel was taken from paper (1). From a comparison of these curves, it can be seen that the region of the no effect of the notch, which was discussed earlier and designated as point N_3, has a value of 389 cycles for steel and is greater than aluminium alloys, which is 194 cycles. Paper (70) suggested

using a value of 500 cycles due to the fact that this is between the recommendations of Schijve (71) of 100, and Lee et al. (2) amounting to 1000. In the present paper, a value of 400 was assumed for aluminium alloys, which corresponds to the mean value of the second part of the distribution shown by the formula 8.

RESULTS

As a result of the high-cycle fatigue life testing of heat-treated and artificially aged AA2519 aluminium alloy, three high-cycle fatigue characteristics were obtained. The first is for specimens shaped without a notch, while the next two are for specimens with a rounding in the roof of the notch of 1 mm and 2 mm, respectively. Two intersection
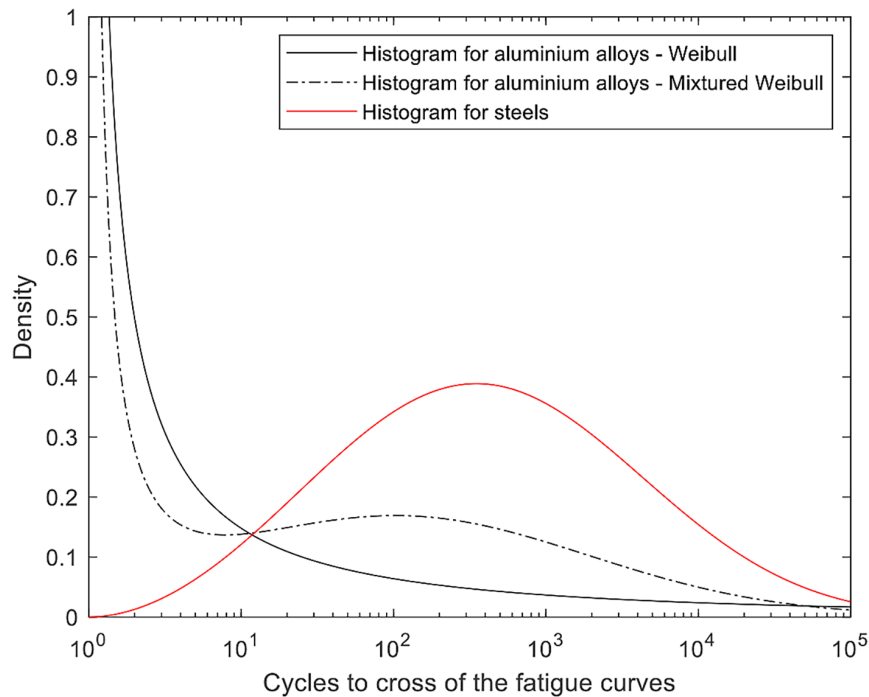
Figure 7. Histogram of fatigue characteristic intersection values for aluminum alloys and steel

points of these fatigue curves were also determined. According to the assumptions made, the intersection point marks the region of the effect of the notch for the described AA2519 alloy. The results are shown graphically in Figure 8. The ordinate axis of these diagram shows the nominal stresses expressed on a logarithmic scale. The horizontal axis, on the other hand, presents the number of cycles leading to destruction also expressed on a logarithmic scale. The points at which there is an arrow with the arrowhead pointing to the right are the points for which the experiment was terminated, even when the specimen was not destroyed (marked as runout). It was assumed that the "fatigue limit" was reached at this nominal stress level. It should be noted that the described situation occurred only for smooth specimens. In addition, the diagram includes the mixtured Weibull probability distribution extensively described in Section 3. The obtained values of the number of cycles at the intersection of the fatigue characteristic curves for different notch geometries (61 – for $r_2 = 1$ mm, 854 – for $r_1 = 2$ mm) occurred around the expected values of the second term of the distribution of the formula (4).

The test specimens were subjected to cyclic loading which, in almost all cases, led to failure understood as the separation of the individual parts of the test object. As shown, depending on the notch, the specimens tested differed significantly in durability. Therefore, it was decided to analyse the shape of the fracture of the specimens to find the relationship between notch geometry and durability. For this purpose, a Keyence VHX-7000 optical laboratory microscope with the ability to optically measure fracture topography was used. Selected recorded images for the analysed specimens for each notch geometry are presented in Fig. 9. The fracture test specimens were selected in such a way that despite the different nominal stress values, the optically analysed specimens showed the same durability. In simple terms, it can be said that the specimens analysed were those whose durability in the form of points is located in the middle part of the *S-N* diagram. It should be noted that the axis of the camera lens was oriented parallel to the initial axis of symmetry of the specimen, and the obtained isometric character of the surface image is solely the result of digital image processing. Therefore, one should not succumb to the conviction that the lens was pointed at an angle other than 90° to the surface of the fracture.

Based on the analysis of the topography of the recorded fractures, it is difficult to clearly determine the mode of failure and determine the relationship of notch geometry to durability. In contrast, it can be seen that in most cases the site of crack initiation is located in one of the
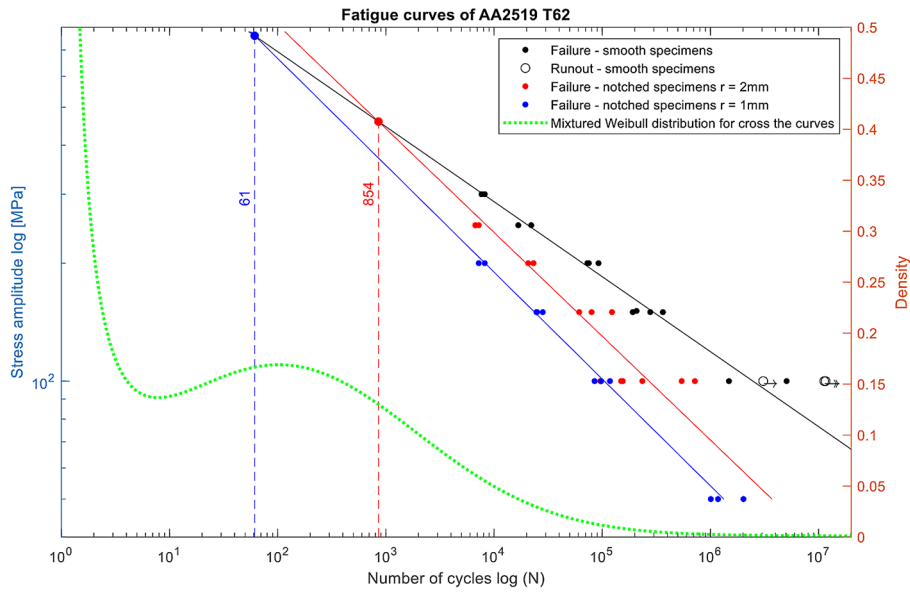
Figure 8. Comparison of nominal stress – number of cycles curves of AA2519 T62 aluminium alloy for smooth and notched specimens *(r₁ = 2* mm and *r₂ = 1* mm) with indication of characteristic intersection and Weibull probability distribution of occurrence of described intersection (as described in section 3)

corners of the specimen. In addition, the fractures of specimens with notches of 1 mm and 2 mm radius break in this way. The similarity lies in the formation of two planes in the fracture, which are at a different height. Slightly different is the case of smooth specimens, where you can very clearly see the crack focus which propagates until a fracture is formed. Finally, the shape of the fracture for smooth specimens is topographically much less complex than for notched specimens. The occurrence of opposite nesting of crack origins in some fractures is most likely due to the fact that when a crack is initiated, a bending moment appears in one of the corners caused by a shift in the axis of load action with respect to the symmetry axis of the specimen. The increased unilateral susceptibility of the specimen resulted in a complex loading condition at the opposite end of the specimen, which produced a secondary crack focus. Subsequent loading cycles led to the propagation of already existing cracks. This phenomenon is particularly evident in Figures 9a, 9c, and 9d.

PROPOSAL OF AUTHOR'S OWN ANALYTICAL-EXPERIMENTAL METHOD AND ITS VERIFICATION

To describe the results of high-cycle fatigue tests, the Basquin equation is most often used according to the following relationship:

$$\log(N) = m_w \cdot \log(S_a) + b \qquad (9)$$

where: m_w – directional coefficient, b – absolute term.

Knowing the characteristics of smooth specimens, it is possible to determine the characteristics of notched specimens according to the following procedure. To determine the directional coefficient of the *S-N* curve for notched specimens, the relationship after transformation of the formula (9) can be used, taking the values of the points from Figure 1. Then the directional coefficient is (1):

$$m_w = \frac{\log\left(\frac{N_Z}{N_3}\right)}{log\left(\frac{0.9R_m}{S_{f6}}\right)} \qquad (10)$$

where: N_Z – base number of cycles $2 \cdot 10^6$, S_{f6} – "fatigue limit" for a structural member calculated after Smith and Miller (72) according to the following relation:

$$S_{f6} = \frac{Z}{K_t} \qquad (11)$$

The formula (11) can be used for (1):

$$K_t \cdot Z < 1.1R_{p0.2} \qquad (12)$$

Analytical and experimental characteristics obtained according to the method described above are shown in Figure 10. On the other hand, the
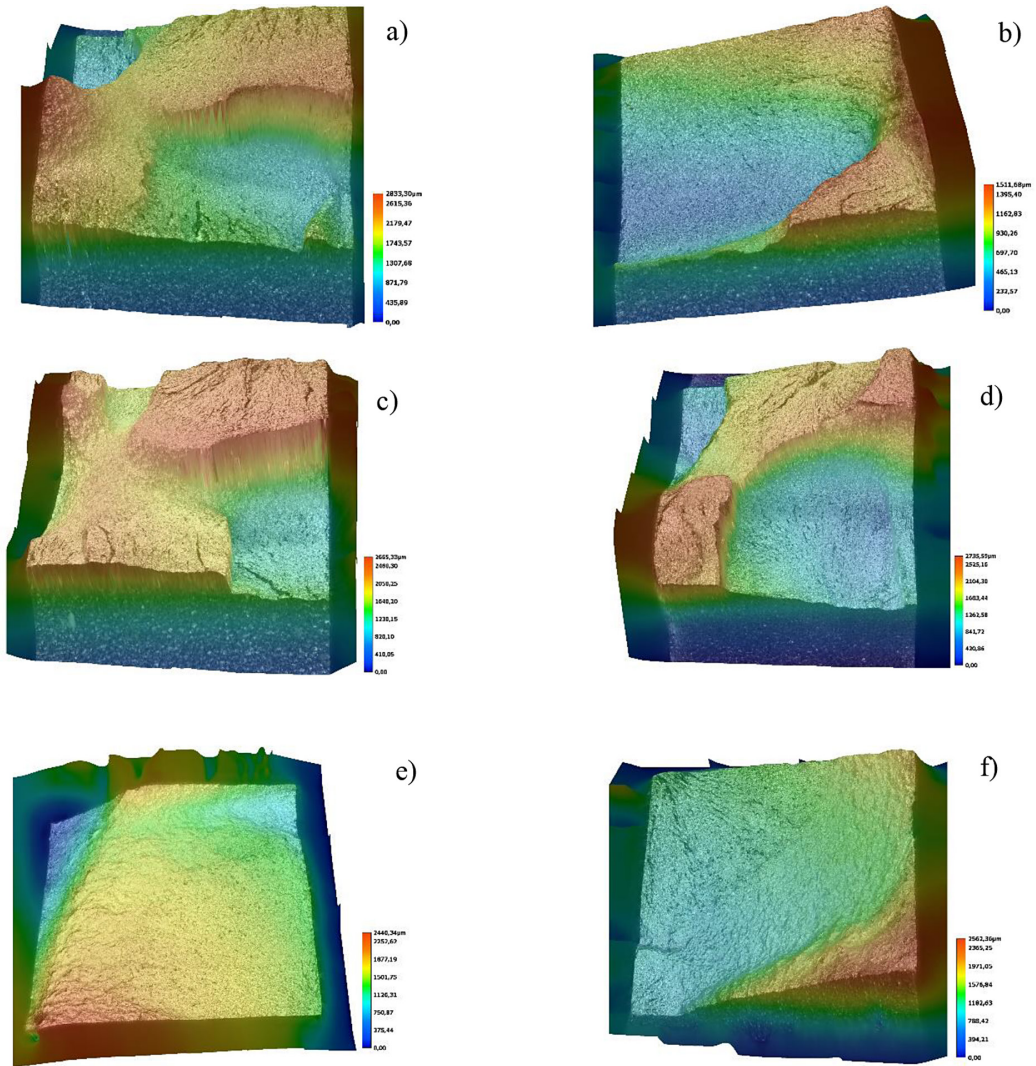
Figure 9. Comparison of topography of selected fractures of specimens with different notch bottom rounding radii, a) $r_2 = 1$ mm $\sigma_N = 100$ MPa, b) $r_2 = 1$ mm, $\sigma_N = 50$ MPa, c) $r_1 = 2$, $\sigma_N = 150$ MPa, d) $r_1 = 2$ mm, $\sigma_N = 100$ MPa, e) $r = 20$ mm, $\sigma_N = 150$ MPa, f) $r = 20$ mm, $\sigma_N = 150$ MPa
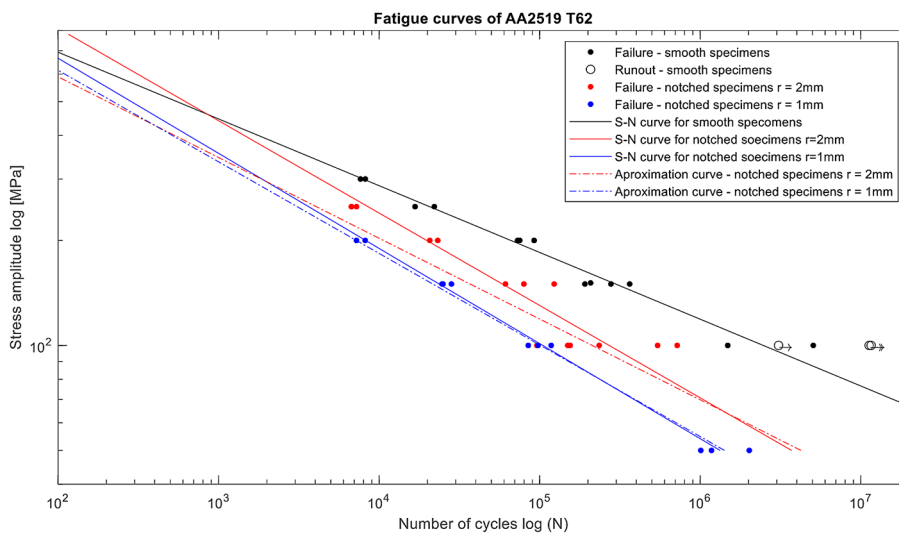
Figure 10. Fatigue diagram for AA2519 T62 aluminium alloy for smooth and notched specimens ($r_1 = 2$ mm and $r_2 = 1$ mm) showing the intersection of characteristics and the proposal method

ANALYTICAL-EXPERIMENTAL METHOD
DETERMINE S-N CURVE FOR STRUCTURAL ELEMENT

Enter parameters of the material
- from tensile test – R_m and $R_{p0.2}$
- from fatigue tests – Z, N_Z (can be assume $2 \cdot 10^6$)

Calculate stress intensity factor K_t

Is relation $K_t \cdot Z < 1.1 R_{p0.2}$. fulfil?

No → Fatigue test for the structural element must be perform

Yes

Calculate "fatigue limit" for a structural element:
$$S_{f6} = \frac{Z}{K_t}.$$

Calculate the slope coefficient of the S-N curve for structural element ($N_3 = \sim 400$ cycles):
$$m_w = \frac{\log\left(\frac{N_Z}{N_3}\right)}{log\left(\frac{0.9R_m}{S_{f6}}\right)}$$

Calculate intercept of the S-N curve for structural element:
$$b = \frac{\log(10^3)}{m_w \cdot \log(S_3)}.$$

Fatigue life estimate by eq.:
$$\log(N) = m_w \cdot \log(S_a) + b$$

Figure 11. The computational algorithm for proposed analytical-experimental method

comparison between the values obtained according to the proposed methodology and the experimental values is shown in Figure 14.

Additionally, verification was performed too for the Lee and Taylor method (2) and FITNET method (8). Fatigue characteristics for these methods were presented in Figure 12 and Figure 13. *S-N* curve for smooth specimens were estimated from tensile test results (ultimate strength). To quality errors made by each method, a diagram of the number of experiments and estimated cycles was made. Figures 14–16 present the diagrams for each method separately. The estimated fatigue life by the proposed method was in a scatter band equal to 3 (except for two points
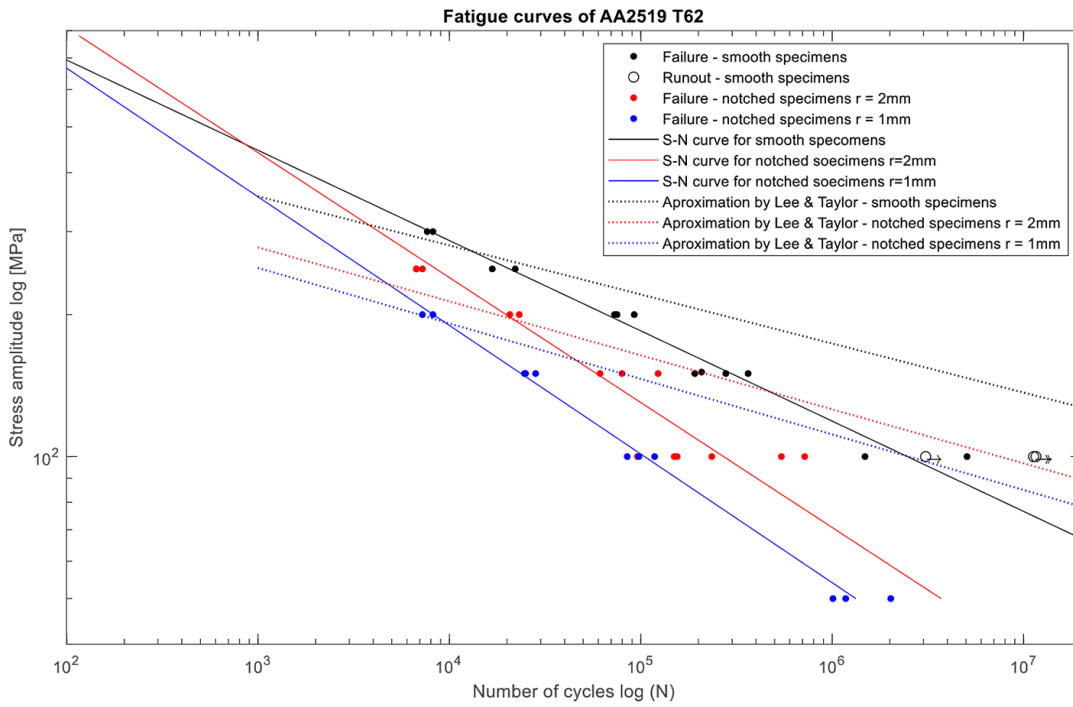
Figure 12. Fatigue diagram for AA2519 T62 aluminium alloy for smooth and notched specimens (r_1 = 2 mm and r_2 = 1 mm) showing intersection of characteristics and Lee and Taylor method
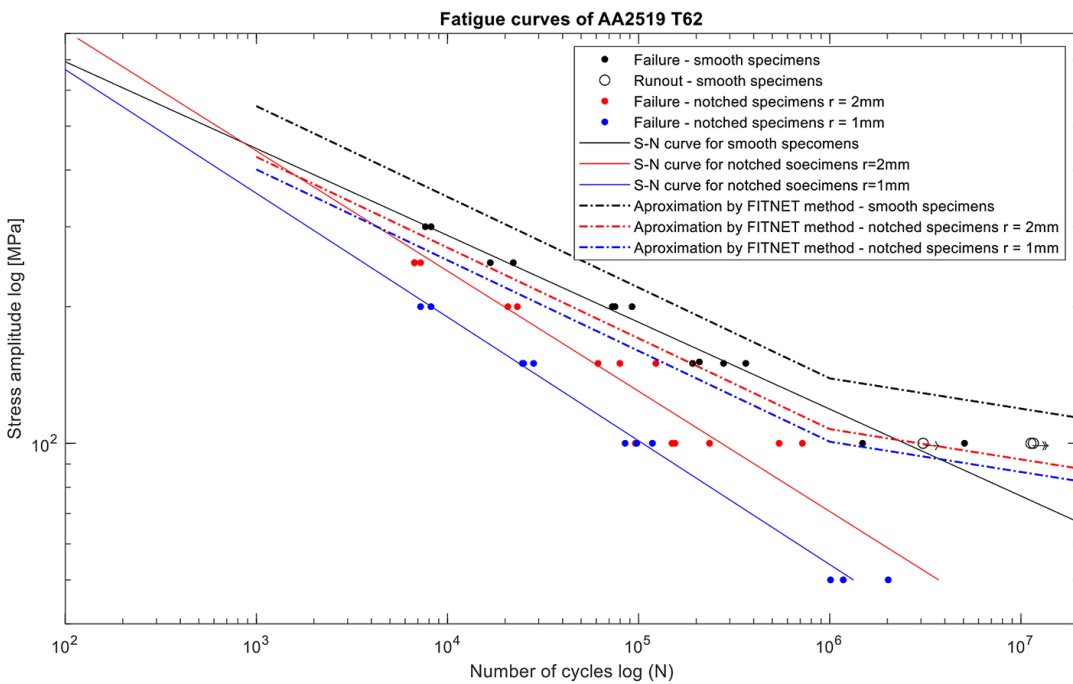
Figure 13. Fatigue diagram for AA2519 T62 aluminium alloy for smooth and notched specimens (r_1 = 2 mm and r_2 = 1 mm) showing intersection of characteristics and FITNET method

for specimens with radii of 2 mm, but they were on the safety part). However, Lee and Taylor's method only for less than 10^5 cycles in the scatter band. For fatigue life higher than 10^5 cycles it was overestimated. Similar situation was for FITNET method,

but for specimens with radii 1 mm overestimated values were for all. For quantity verification a criterium of quantity of the model can be formulated as: a model M should be chosen from under consideration of models in such a way that the model output
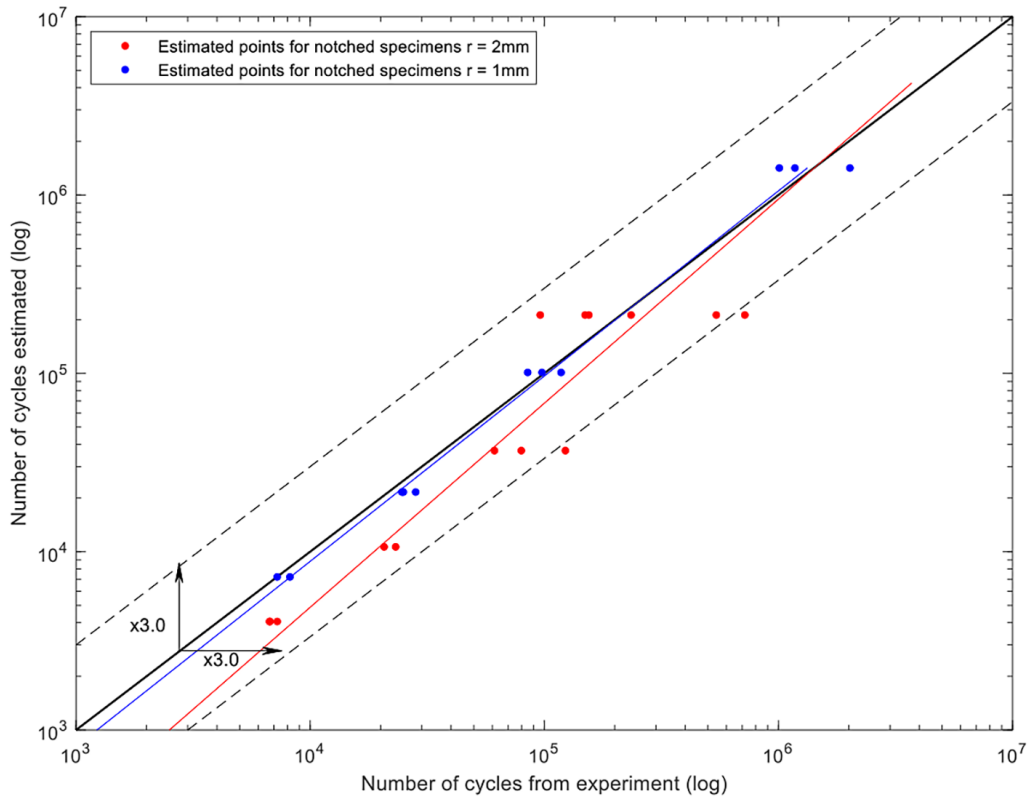
Figure 14. The comparison between the values obtained according to the proposed methodology and the experimental values for AA2519 T62 aluminium alloy
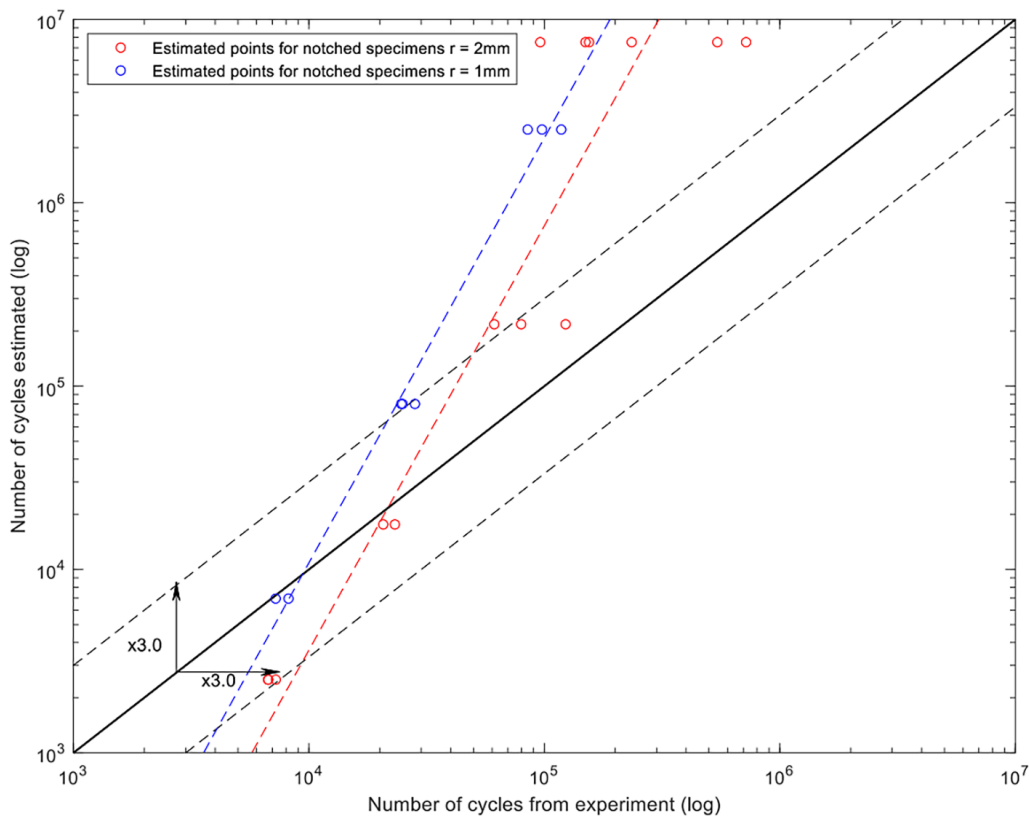
Figure 15. The comparison between the values obtained according to the Lee and Taylor methodology and the experimental values for AA2519 T62 aluminium alloy
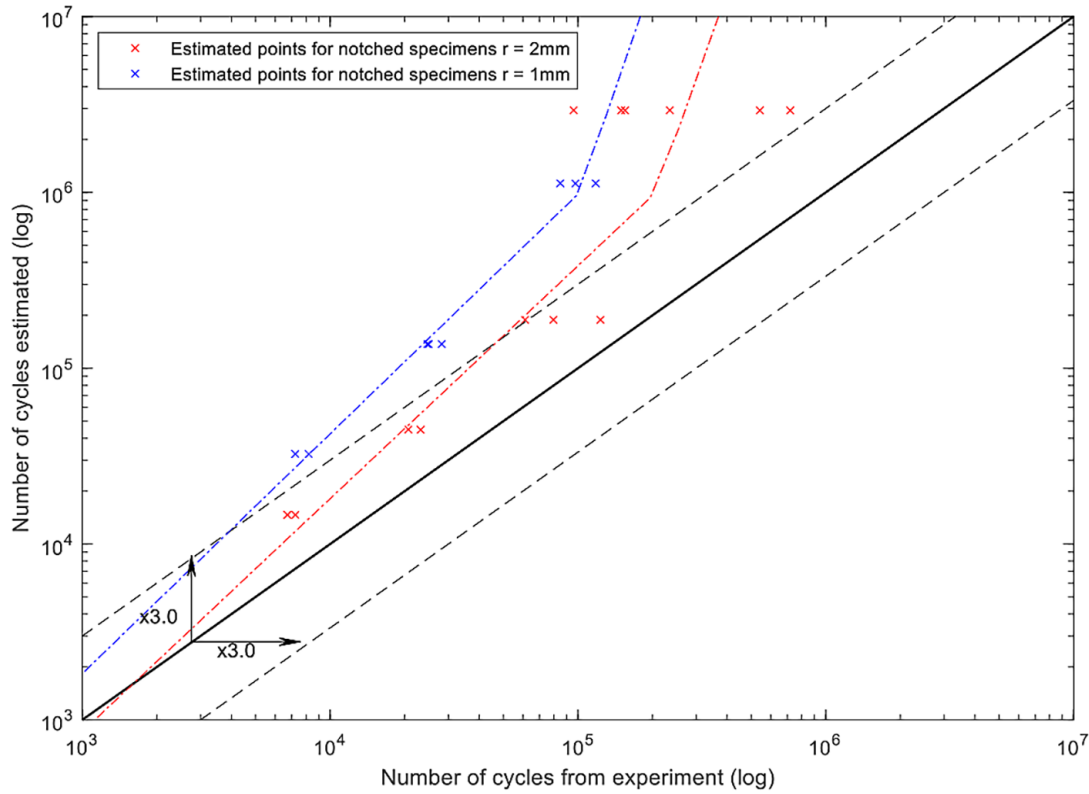
Figure 16. The comparison between the values obtained according to the FITNET methodology and the experimental values for AA2519 T62 aluminium alloy

X_M contains maximum information (in the Shannon sense (73)) about the real system output X, that is:

$$Q(X, X_M) = \iint f(x, x_M) \log \left(\frac{f(x|x_M)}{f(x)} \right) dx dx_M \to max \quad (13)$$

When it can be assumed that distribution for model and real system output are normals it becomes:

$$Q(X, X_M) = -\frac{1}{2} \log(1 - \rho^2) \quad (14)$$

where:

$$\rho = \frac{cov(X, X_M)}{\sigma_x \sigma_{x_M}} \quad (15)$$

$$cov(X, X_M) = E(X \cdot X_M) - E\big(E(X) \cdot E(X_M)\big) \quad (16)$$

Results of calculations for analysing models (the proposed method, FITNET and Lee and Taylor) are presented in Table 5. The highest values are bolded.

DISCUSSION

The presented analysis of the value of the number of cycles of N_3 for which there is no effect of notch on the high-cycle fatigue life for

Table 5. Values of the criterium of quantity of the models

Model	$Q(X, X_M)$	
	$r = 1$ mm	$r = 2$ mm
Proposed model	2.312	1.030
FITNET	1.016	0.293
Lee and Taylor	1.017	0.290

aluminium alloy showed that there is such a range. The obtained values of the limiting number of cycles are smaller than for steel according to papers (1, 70). Note that the values obtained for the aluminium alloy are bi-modal, unlike those obtained for steel. For this reason, a mixtured Weibull distribution was used to describe the distribution of N_3 values. In addition, it can be stated that Łagoda et al. (9) were wrong in stating that for aluminium alloys there is no region of no effect of notch.

Based on the analysis of the literature and the fatigue tests carried out, a model for determining the fatigue characteristics for a structural component based on material characteristics is proposed. The verification results obtained showed that the estimated curves were within 3 times the error.

Better fatigue life estimation results according to the proposed method were obtained for specimens with a notch of $r = 1$ mm with a K_t of 2.28 than for those with a softer notch of $r = 2$ mm.

Additionally, the verification was performed for FITET and Lee and Taylor methods, which have obtained worse results. The FITNET method determines overestimated values for the entire range of test results. Slightly better results were obtained by Lee and Taylor method, where overestimated values occurred after 10^5 cycles. However, the values for the criterium of quantity by these methods were similar. Only the proposed method got the best results for all geometry of the specimens (5).

It should be noted that the proposed method has practical advantages for the designer. This is due to the fact that during the design study, the geometry of the element changes, which changes the value of form factor K_t. Because of this, fatigue damage can occur, for example, through a change in the radius of the conveyor shaft's step transition that occurred during the manufacturing process (74). In order not to perform fatigue tests for each geometry considered, analytical methods presented in the literature, for example, in (1, 2, 8, 71) are used.

Analysis of the fracture topography shows that the notch geometry affects the fracture mechanism and the shape of the fracture. The accumulation of stresses in the roof of the notch increases the variation in the height of irregularities distributed evenly across the entire fracture surface. No such variation was observed for smooth specimens.

CONCLUSIONS

The following conclusions have been drawn from the study:
- Based on the obtained results, it was concluded that aluminium alloys should be divided into at least two groups. The first group includes materials that have an expected N_3 value of one load cycle. In contrast, the second group has an expected N_3 value of ~ 400 cycles, which was adopted for the proposed analytical and experimental method.
- The proposed method has got the best results of verification, compared to FITET and Lee and Taylor methods.
- It is worth mentioning that the obtained values for the proposed method were on the safety region.

- Greater accuracy in estimating fatigue characteristics can be obtained using the analytical-experimental method presented in this paper. The resulting estimation error can be considered satisfactory.

REFERENCES

1. Strzelecki P. Analytical method for determining fatigue properties of materials and construction elements in high cycle life (in Polish). [Bydgoszcz]: Uniwersytet Technologiczno-Przyrodniczy w Bydgoszczy. 2014.

2. Lee YL, Paw J, Hathaway, Richard B, Barkey, Mark E. Fatigue Testing and Analysis - Theory and Practice. Elsevier Butterworth–Heinemann. 2005; 417.

3. Fatemi A, Zeng Z, Plaseied A. Fatigue behavior and life predictions of notched specimens made of QT and forged microalloyed steels. Int J Fatigue. 2004; 26: 663–72.

4. Strzelecki P, Correia JA, Sempruch J. Estimation of fatigue S-N curves for aluminium based on tensile strength – proposed method. MATEC Web of Conferences. 2021; 338: 01026.

5. Seyda J, Skibicki D, Pejkowski Ł, Skibicki A, Domanowski P, Maćkowiak P. Mechanical properties and microscopic analysis of sintered rhenium subjected to monotonic tension and uniaxial fatigue. Materials Science and Engineering A. 2021; 817.

6. Bannantine JA, Comer JJ, Handrock JL. Fundamentals of metal fatigue analysis. 1st ed. New Jersey: Pearson. 1989; 288.

7. Stephens RR, Stephens RI, Fuchs HO, Fatemi A. Metal fatigue in engineering. Journal of Engineering Materials and Technology. John Wiley and Sons. 2001; 34.

8. Kocak M, Webster S, Janosch JJ, Ainsworth, RA, Koers R. FITNET Fitness-for-service procedure – final draft MK7. 2006.

9. Łagoda T, Robak G, Słowik J. Fatigue life of steel notched elements including the complex stress state. Mater Des [Internet]. 2013 Oct;51:935–42. Available from: https://linkinghub.elsevier.com/retrieve/pii/S026130691300410X

10. Duparc OH. Alfred Wilm et les débuts du Duralumin. Revue de Metallurgie Cahiers D'Informations Techniques. 2004; 101(5): 353–60.

11. Boroński D, Dzioba I, Kotyk M, Krampikowska A, Pala R. Investigation of the fracture process of explosively welded AA2519-AA1050-Ti6Al4V layered material. Materials [Internet]. 2020 May 13 [cited 2020 Jun 23]; 13(10): 2226. Available from: https://www.mdpi.com/1996-1944/13/10/2226

12. Fisher JJ, Kramer LS, Pickens JR. Aluminum alloy

2519 in military vehicles. Advanced Materials and Processes. 2002; 160(9): 43–6.

13. Kramer LS, Blair TP, Blough SD, Fisher JJ, Pickens JR. Stress-corrosion cracking susceptibility of various product forms of aluminum alloy 2519. J Mater Eng Perform [Internet]. 2002 [cited 2017 Jun 16]; 11(6): 645–50. Available from: http://search.proquest.com/openview/d391cf047b4289bcf46132ca208897d4/1?pq-origsite=gscholar&cbl=14822

14. Pawel SJ. Scouting tests to examine potential corrosion of aluminum alloy 2519 during fabrication [Internet]. [cited 2017 Jun 16]. Available from: https://www.osti.gov/scitech/biblio/304018-TA0rqQ/webviewable/

15. The Aluminum Association Inc. International Alloy Designations and Chemical Composition Limits for Wrought Aluminum and Wrought Aluminum Alloys. The Aluminum Association, Arlington, Virginia. 2006; (April 2006): 28.

16. Davis JR. Aluminum and Aluminum Alloys. Materials Park, Ohio: ASM Hndbook; 1993. 732 p.

17. Vasudevan AK, Doherty RD. Aluminum Alloys: Contemporary Research and Applications. Academic Press. New York: academic press inc. 1989; 728.

18. Liang XP, Li HZ, Huang L, Hong T, Ma B, Liu Y. Microstructural evolution of 2519-T87 aluminum alloy obliquely impacted by projectile with velocity of 816 m/s. Transactions of Nonferrous Metals Society of China (English Edition) [Internet]. 2012; 22(6): 1270–9. Available from: http://dx.doi.org/10.1016/S1003-6326(11)61315-0

19. Gao H, Zhang XM, Li HZ, Liu Y. Microstructure Inhomogeneities in 2519A Aluminum Plate Penetrated by an Incendiary Projectile. Materials Science Forum. 2007; 546–549: 1049–54.

20. Lin Q, Dong W, Li Y, Zhang H, Wang Z. Microstructure simulation of 2519 aluminum alloy in multipass hot compression process. Procedia Eng. 2014; 81: 1259–64.

21. Starke EA, Staley JT. Application of modern aluminum alloys to aircraft. Progress in Aerospace Sciences. 1996; 32(2–3): 131–72.

22. Kosturek R, Śnieżek L, Grzelak K, Torzewski J. Study on the Weldability of AA2519 Armor Grade Aluminium Alloy. Manufacturing Technology [Internet]. 2021; 21(6): 818–23. Available from: https://doi.org/10.21062/mft.2021.093

23. Kosturek R, Śnieżek L, Torzewski J, Wachowski M. Research on the friction stir welding of Sc-modified AA2519 extrusion. Metals (Basel). 2019; 9(10).

24. Kozmel T, Vural M, Tin S. EBSD characterization of shear band formation in aluminum armor alloys. J Mater Sci. 2016; 51(16): 7554–70.

25. Da-xiang S, Xin-ming Z, Ling-ying Y, Xing-hui G, Hai-chun J, Gang G. Comparative study of the dynamic mechanical behavior of aluminum alloy 2519A and 7039. Materials Science and Engineering A [Internet]. 2015; 640: 165–70. Available from: http://dx.doi.org/10.1016/j.msea.2015.05.092

26. Prasad GS, Sharmila T, SrmivasaRao K, Reddy GM. Effect of welding process on microstrnctnre, mechanical properties and corrosion behavior of AA2519 al-alloy. AIP Conf Proc. 2021; 2395(October).

27. Liu Y, Zhang PF, Chen LJ, Zhang H, Zhang XM, Geng ZJ. Effect of pre-precipitation on localized corrosion properties of 2519A aluminum alloy. Cailiao Gongcheng/Journal of Materials Engineering [Internet]. 2014; 6: 11–17. Available from: https://www.scopus.com/inward/record.uri?eid=2-s2.0-84903895163&doi=10.11868%2Fj.issn.1001-4381.2014.06.003&partnerID=40&md5=113ba42821b5c8904f063fe9e7b95f1d

28. Ye LY, Wu YP, Jia YZ, Zhang XM, Wu GL. Effects of secondary aging on microstructure and properties of 2519A aluminum alloy. Zhongguo Youse Jinshu Xuebao/Chinese Journal of Nonferrous Metals [Internet]. 2014; 24(3): 624–630. Available from: https://www.scopus.com/inward/record.uri?eid=2-s2.0-84899732593&partnerID=40&md5=cc8d10a1aa03cbdfe5f43400a5b6a86d

29. Li HZ, Liang XP, Wei XY, Wang HJ, Liu HT, Guo FF. Effect of quenching agent on intergranular corrosion resistance of 2519 aluminum alloy. Fenmo Yejin Cailiao Kexue yu Gongcheng/Materials Science and Engineering of Powder Metallurgy [Internet]. 2010; 15(2): 123–128. Available from: https://www.scopus.com/inward/record.uri?eid=2-s2.0-77953729826&partnerID=40&md5=68068fc61b723ce100a040ebe3b6d706

30. Chen M an, Liu S ying, Li J ming, Cheng N, Zhang X ming. Improvement to corrosion resistance of MAO coated 2519 aluminum alloy by formation of polypropylene film on its surface. Surf Coat Technol [Internet]. 2013; 232: 674–9. Available from: http://dx.doi.org/10.1016/j.surfcoat.2013.06.073

31. Liu Y, Zhang XM, Zhang H. Role of secondary phase particles of 2519A aluminium alloy in localised corrosion. Materials Research Innovations. 2013; 17(1).

32. Kravcov A, Kluczyński J, Kosturek R, Franek O, Morozov N, Śnieżek L, Svoboda P, Kubeček P. The influence of friction stir welded process parameters of AA2519-T62 on joint quality defined by non-destructive laser amplified ultrasonic method and by microstructure analysis. Challenges to National Defence in Contemporary Geopolitical Situation. 2020; 2020(1): 74–8.

33. Kravcov A, Kosturek R, Śnieżek L, Kluczyński J, Franek O, Morozov N, Maciejewski P. The influence of friction stir welded process parameters of

AA2519-T62 on joint quality defined by non-destructive laser amplified ultrasonic method and by microstructure analysis. Acta Polytechnica. 2020; 60(5): 415–9.

34. Sabari SS, Malarvizhi S, Balasubramanian V. Influences of tool traverse speed on tensile properties of air cooled and water cooled friction stir welded AA2519-T87 aluminium alloy joints. J Mater Process Technol [Internet]. 2016; 237: 286–300. Available from: http://dx.doi.org/10.1016/j.jmatprotec.2016.06.015

35. Sree Sabari S, Malarvizhi S, Balasubramanian V. Characteristics of FSW and UWFSW joints of AA2519-T87 aluminium alloy: Effect of tool rotation speed. J Manuf Process [Internet]. 2016; 22: 278–89. Available from: http://dx.doi.org/10.1016/j.jmapro.2016.03.014

36. Płonka B, Rajda M, Zamkotowicz Z, Zelechowski J, Remsak K, Korczak P, Szymański W, Śnieżek I. Studies of the aa2519 alloy hot rolling process and cladding with en aw-1050a alloy. Archives of Metallurgy and Materials. 2016; 61(1): 381–8.

37. Zuiko I, Kaibyshev R. Deformation structures and strengthening mechanisms in an Al-Cu alloy subjected to extensive cold rolling. Materials Science and Engineering A. 2017 Aug 15; 702: 53–64.

38. Sun D, Gu G, Ye L, Zhang X. Effect of cold deformation and reaging on microstructures and mechanical properties of 2519A-T87 alloy plate. Zhongnan Daxue Xuebao (Ziran Kexue Ban)/Journal of Central South University (Science and Technology). 2014; 45(12): 4145–4151.

39. Wu YP, Ye LY, Jia YZ, Liu L, Zhang XM. Precipitation kinetics of 2519A aluminum alloy based on aging curves and DSC analysis. Transactions of Nonferrous Metals Society of China (English Edition). 2014; 24(10): 3076–83.

40. Liu Y, Cheng R, Wang J, Zhang H, Zhang X. Effect of severe plastic deformation at ambient temperature onmicrostructures and mechanical properties of aluminum alloy 2519. Materials Science Forum. 2013; 745–746: 298–302.

41. Zhang XM, Liu L, Ye LY, Liu J, Lei Z, Song JC. Effect of pre-deformation of rolling combined with stretching on stress corrosion of aluminum alloy 2519A plate. Transactions of Nonferrous Metals Society of China (English Edition). 2012; 22(1): 8–15.

42. Wang HM, Xia CQ, Lei P, Wang ZW. Influence of thermomechanical aging on microstructure and mechanical properties of 2519A aluminum alloy. Journal of Central South University of Technology (English Edition). 2011; 18(5): 1349–1353.

43. Wang HM, Xia CQ, Wu LR, Zhou F. Effect of aging temperature on microstructure and mechanical properties of cold-heavy deformed 2519A aluminum alloy. Cailiao Rechuli Xuebao/Transactions of

Materials and Heat Treatment. 2011; 32(6): 83–86.

44. Li HZ, Wang HJ, Liang XP, Liu HT, Liu Y, Zhang XM. Hot deformation and processing map of 2519A aluminum alloy. Materials Science and Engineering A. 2011; 528(3): 1548–52.

45. Wang H, Xia C, Lei P, Wang Z. Observation of precipitation phase in thermo-mechanical ageing 2519A aluminum alloy. Tezhong Zhuzao Ji Youse Hejin/Special Casting and Nonferrous Alloys. 2010; 30(11): 1040–1042.

46. Zhang XM, Liu L, Jia YZ. Effects of stretching and rolling pre-deformation on microstructures and mechanical properties of 2519A aluminum alloy. Zhongguo Youse Jinshu Xuebao/Chinese Journal of Nonferrous Metals. 2010; 20(6): 1088–1094.

47. Haynes MJ, Gangloff RP. Elevated temperature fracture toughness of Al-Cu-Mg-Ag sheet: Characterization and modeling. Metall Mater Trans A Phys Metall Mater Sci. 1997; 28(9): 1815–29.

48. Kotyk M, Boroński D, Maćkowiak P. The influence of cryogenic conditions on the process of AA2519 aluminum alloy cracking. Materials. 2020; 13(7).

49. Gangloff RP, Haviland JK, Herakovich CT, Pilkey WD, Pindera MJ, Thornton EA, Stoner GE, Swanson RE, Wawner FE, Wert JA. NASA-UVA light aerospace alloy and structures technology program [Internet]. Virginia; 1989 Aug [cited 2020 May 29]. Available from: https://ntrs.nasa.gov/search.jsp?R=19910005161

50. Kosturek R, Torzewski J, Joska Z, Wachowski M, Śnieżek L. The influence of tool rotation speed on the low-cycle fatigue behavior of AA2519-T62 friction stir welded butt joints. Eng Fail Anal. 2022; 142(July).

51. Kosturek R, Slezak T, Torzewski J, Wachowski M, Sniezek L. Study on tensile and fatigue failure in the low-hardness zone of AA2519-T62 FSW joint. Manuf Rev (Les Ulis). 2022; 9.

52. Kosturek R, Śnieżek L, Torzewski J, Ślęzak T, Wachowski M, Szachogłuchowicz I. Research on the properties and low cycle fatigue of Sc-modified AA2519-T62 FSW joint. Materials. 2020; 13(22): 1–18.

53. Kosturek R, Śniezek L, Torzewski J, Wachowski M. Low cycle fatigue properties of sc-modified AA2519-T62 extrusion. Materials. 2020; 13(1).

54. Owolabi GM, Thom M, Ajide O, Kumar N, Azimi A, Whitworth H, Warner G. Fatigue Responses of Three AA2000 Series Aluminum Alloys. Journal of Materials Science and Chemical Engineering. 2019; 7(3): 32–48.

55. ISO 1099:2017 - Metallic materials — Fatigue testing — Axial force-controlled method. Genewa: International Organization for Standardization; 2017.

56. Noda N. Stress concentration factors for round and flat test specimens with notches. International Journal of Fatigue. 1995; 17: 163–78.

57. Antunes AMBS, Baptista CARP, Barboza MJR, Carvalho ALM, Mogili NVV. Effect of the interrupted aging heat treatment T6I4 on the tensile properties and fatigue resistance of AA7050 alloy. Journal of the Brazilian Society of Mechanical Sciences and Engineering [Internet]. 2019; 41(8): 1–13. Available from: https://doi.org/10.1007/s40430-019-1821-9

58. Benedetti M, Fontanari V, Santus C, Bandini M. Notch fatigue behaviour of shot peened high-strength aluminium alloys: Experiments and predictions using a critical distance method. Int J Fatigue [Internet]. 2010; 32(10): 1600–11. Available from: http://dx.doi.org/10.1016/j.ijfatigue.2010.02.012

59. Chaves V, Beretta G, Balbín JA, Navarro A. Fatigue life and crack growth direction in 7075-T6 aluminium alloy specimens with a circular hole under biaxial loading. Int J Fatigue [Internet]. 2019; 125: 222–36. Available from: https://doi.org/10.1016/j.ijfatigue.2019.03.031

60. Grover HJ, Gordon SA, Jackson LR. The Fatigue of Metals and Structures. 1954.

61. Illg W. Fatigue Tests on Notched and Unnotched Sheet Specimens of 2024 -T3 and 7075 -T6 Aluminum Alloys and of Sae 4130 Steel With Special Consideration of the Life Range From 2 To 10,000 Cycles. Journal of Wound, Ostomy and Continence Nursing [Internet]. 1956; 16(6): 1–41. Available from: https://ntrs.nasa.gov/archive/nasa/casi.ntrs.nasa.gov/19930084699.pdf%5Cnhttp://content.wkhealth.com/linkback/openurl?sid=WKPTLP:landingpage&an=00152192-198911000-00004

62. Papuga J, Karkulín A, Hanžl O, Lutovinov M. Comparison of several methods for the notch effect quantification on specimens from 2124-T851 aluminum alloy. Procedia Structural Integrity [Internet]. 2019; 19: 405–14. Available from: https://doi.org/10.1016/j.prostr.2019.12.044

63. Strzelecki P. Scatter of fatigue life regarding stress concentration factor. Procedia Structural Integrity [Internet]. 2018; 13: 631–5. Available from: https://linkinghub.elsevier.com/retrieve/pii/S2452321618303391

64. Bennett JA, Weinberg JG. Fatigue notch sensitivity of some aluminum alloys. J Res Natl Bur Stand (1934). 1954; 52(5): 235.

65. Górecki T. Podstawy statystyki z przykladami w R. Wydawnictwo BTC. 2011; 53.

66. Kamys B. Statystyczne Metody Opracowania Pomiarów II. 2007.

67. Rami H, Drissi El Maliani A, El Hassouni M. A Finite Mixture of Weibull-Based Statistical Model for Texture Retrieval in the Complex Wavelet Domain. IEEE Access. 2019; 7: 130144–55.

68. Amalia Yunia Rahmawati. Find minimum of function using genetic algorithm [Internet]. 2020; 1–23. Available from: https://www.mathworks.com/help/gads/ga.html

69. Alan A. An introduction to categorical data analysis. Second Edi. Statistics in Medicine. New Jersey: John Wiley & Sons, Inc.. 2007; 372.

70. Sempruch J, Strzelecki P, Borowski S, editors. Problemy Rozwoju Maszyn Roboczych. Bydgoszcz: Wydawnictwa Uczelniane Politechnika Bydgoska. 2023; 250.

71. Schijve J. Fatigue of structures and materials. Second. Fatigue of Structures and Materials. Springer Science+Business Media. 2009; 377–380.

72. Smith RA, Miller KJ. Fatigue cracks at notches. Int J Mech Sci. 1977; 19(1): 11–22.

73. Sobczyk K, Spencer BF. Random Fatigue. Random Fatigue. London: Academic Press; 1992.

74. van Zyl G, Al-Sahli A. Failure analysis of conveyor pulley shaft. Case Stud Eng Fail Anal [Internet]. 2013 Apr; 1(2): 144–55. Available from: http://dx.doi.org/10.1016/j.csefa.2013.04.011